Role of surface and subsurface processes in scaling N_2O emissions along riverine networks

Alessandra Marzadri[a,1,2], Martha M. Dee[b,1], Daniele Tonina[a,1], Alberto Bellin[c,1], and Jennifer L. Tank[b,1]

[a]Center for Ecohydraulics Research, University of Idaho, Boise, ID 83702; [b]Department of Biological Sciences, University of Notre Dame, Notre Dame, IN 46556; and [c]Department of Civil, Environmental and Mechanical Engineering, University of Trento, Trento 38123, Italy

Edited by Andrea Rinaldo, Laboratory of Ecohydrology, Ecole Polytechnique Federale Lausanne, Lausanne, Switzerland, and approved March 16, 2017 (received for review October 20, 2016)

Riverine environments, such as streams and rivers, have been reported as sources of the potent greenhouse gas nitrous oxide (N_2O) to the atmosphere mainly via microbially mediated denitrification. Our limited understanding of the relative roles of the near-surface streambed sediment (hyporheic zone), benthic, and water column zones in controlling N_2O production precludes predictions of N_2O emissions along riverine networks. Here, we analyze N_2O emissions from streams and rivers worldwide of different sizes, morphology, land cover, biomes, and climatic conditions. We show that the primary source of N_2O emissions varies with stream and river size and shifts from the hyporheic–benthic zone in headwater streams to the benthic–water column zone in rivers. This analysis reveals that N_2O production is bounded between two N_2O emission potentials: the upper N_2O emission potential results from production within the benthic–hyporheic zone, and the lower N_2O emission potential reflects the production within the benthic–water column zone. By understanding the scaling nature of N_2O production along riverine networks, our framework facilitates predictions of riverine N_2O emissions globally using widely accessible chemical and hydromorphological datasets and thus, quantifies the effect of human activity and natural processes on N_2O production.

riverine networks | greenhouse gas | N_2O | emission scaling law | N_2O emission potentials

Riverine environments, such as streams and rivers, have been identified as hotspots of microbially mediated denitrification, where nitrate (NO_3) is converted to both nitrogen gas (N_2), which constitutes the majority of Earth's atmosphere, and nitrous oxide (N_2O), the potent greenhouse gas responsible for stratospheric ozone destruction (1). Denitrification has been observed to occur within both bulk-oxic (2) and anoxic environments (3–5) of both benthic (i.e., sediment–water interface) and hyporheic (i.e., near-subsurface) zones of streams and rivers. Whereas the benthic zone is the ecological region of the streambed, where both aquatic fauna and flora can be found (4, 6), the latter is the band of streambed material mainly saturated of stream water (7). The benthic zone is at the interface between water and sediment and the upper boundary of the fluvial hyporheic zone. Current understanding suggests that riverine N_2O production occurs predominantly in these two environments, reflecting two distinct biogeochemical transformation zones (6), irrespective of system size from headwater streams to rivers. The produced N_2O is then exchanged with the atmosphere through diffusive evasion, with dynamics that depend on N_2O concentrations of the water in relation to atmospheric equilibrium (6, 8), stream hydrodynamics, temperature, and the air–water gas exchange rate (9). Although it is understood that microbially mediated denitrification is responsible for a large proportion of N_2O production in riverine networks (6, 10, 11), quantifying these emissions is challenging because of a lack of high-resolution field data and inadequate parameterization of the dominant biogeochemical processes responsible for N_2O production at scales ranging from the individual reach to the river network. In addition to the uncertainty associated with predictions of N_2O emissions from streams and rivers, recent studies suggest that global emissions from riverine networks presented in the most recent Intergovernmental Panel on Climate Change report are likely underestimated (6, 12–14). This uncertainty results in part from the dependence of biogeochemical reactions on complex interactions occurring at the reach scale among the water column, benthic, and hyporheic zones. A key factor, which has been elusive in previous works, is the identification of a scaling relationship that allows us to upscale processes occurring within a single reach to best quantify emissions at the riverine network scale. This scaling relationship is needed to improve climate change models that account for anthropogenic activities and natural processes on streams and rivers and the consequent N_2O emission from these systems.

Here, we identify and define this scaling law by linking, through a model, N_2O emissions with geomorphic, hydrodynamic, and biogeochemical characteristics of streams and rivers and their hyporheic zones, thereby proposing a methodology to upscale reach-scale processes to riverine networks globally. Our model identifies the primary hydrodynamics and biogeochemical processes responsible for N_2O emissions from streams and rivers. Hydrodynamics controls the delivery of reactants to microbial assemblages and determines residence times for reactions to occur (5, 15–17), whereas solute availability and biogeochemical activity drive the conversion of solutes to gasses. This analysis shows that N_2O production per unit of stream/river surface area from the river network worldwide is bounded between two N_2O emission potentials: the upper N_2O emission potential is caused by production within the benthic–hyporheic interface, and the lower N_2O emission potential is caused by production within the benthic–water column zone. These two limits emerge, because N_2O emissions per unit area reduce moving downstream from streams to rivers because of the systematic reduction of the hyporheic contribution, which is only partially compensated by the increase of the contribution from the water column (4, 12, 18). We assumed that

Significance

We show that N_2O emissions from riverine systems depend on river and stream size and that the primary source of N_2O production shifts from the hyporheic and benthic zones in streams to the benthic and water column in rivers. This analysis also reveals the primary scaling factors governing riverine N_2O emissions. Finally, it provides a predictive tool to quantify N_2O emissions from any riverine environment worldwide, among biomes, land-use types, and climatic conditions, using readily available reach-scale biogeochemical measurements and hydromorphological data.

Author contributions: A.M., M.M.D., D.T., A.B., and J.L.T. designed research; A.M., D.T., and A.B. performed research; M.M.D. and J.L.T. analyzed data; M.M.D. and J.L.T. established synoptic sampling protocols and measurements; and A.M., M.M.D., D.T., A.B., and J.L.T. wrote the paper.

The authors declare no conflict of interest.

This article is a PNAS Direct Submission.

[1]A.M., M.M.D., D.T., A.B., and J.L.T. contributed equally to this work.

[2]To whom correspondence should be addressed. Email: amarzadri@uidaho.edu.

This article contains supporting information online at www.pnas.org/lookup/suppl/doi:10.1073/pnas.1617454114/-/DCSupplemental.

ammonium entering via groundwater, or other routes, is quickly nitrified, such that in-stream processes (i.e., hyporheic zone, benthic, and water column) are the primary source of N_2O emissions, whereas direct N_2O contribution, which may enter the streams from groundwater or terrestrial origin, is negligible (6).

We unveiled this scaling and developed our model by analyzing available N_2O emission data and hydromorphological parameters of 12 headwater streams in the Kalamazoo River (Michigan) watershed (19, 20) and 16 headwater streams associated with the second Lotic Intersite Nitrogen eXperiment (LINXII) Study (6, 10, 11). These data allow us to parse the relative roles of the benthic and hyporheic zones in N_2O emissions and constrain them between two limits: upper- and lower-bound models. We then validated the scaling law and the identified upper- and lower-bound models with data that we collected during synoptic sampling campaigns along the Tippecanoe River (Indiana) and Manistee River (Michigan) watersheds and data available in the literature collected in a midsized United Kingdom river (21, 22) (Swale-Ouse River), six large river networks in Africa (23) (Athi–Galana–Sabaki, Betsiboka, Congo, Rianila, Tana, and Zambezi), and a large tidal river (24, 25) (Hudson River in New York) (6, 10, 19–25) (descriptions of these streams are in Tables S1, S2, and S3). These streams are more than 400 testing reaches with contrasting land use land cover (LULC), biomes, climatic conditions, morphology, and size (Table S4).

Results and Discussion

Analysis of average flux of N_2O emissions per unit area, FN_2O (micrograms N per square meter per hour), from the study reaches of all of 417 analyzed streams and rivers to the atmosphere shows that FN_2O systematically decreases with system size (as width) along a gradient from headwater streams to rivers (Fig. 1) of contrasting river networks (e.g., US streams and African rivers) and within the same networks (e.g., Manistee and Tippecanoe, with channel widths that span <1 to >50 m) (Table S2). Using this analysis, streams and rivers can be classified in three zones according to the gradient of reduction in emissions shown in Fig. 1. Zone 1, which includes small streams with widths (W) that are less than 10 m (4), shows a very steep reduction of emissions with stream size. Zone 2, which includes streams with $10 < W < 30$ m, has a gradual reduction of emissions with stream size, and zone 3 groups rivers with $W \geq 30$ m and N_2O emissions that do not depend on W. These proposed breaks are similar to those reported in the stream geomorphological literature (26, 27), suggesting the importance of stream hydromorphological characteristics for determining the biogeochemistry of streams/rivers (details are in *SI Text*). We hypothesized that this reduction is caused by a shift from N_2O production that occurs primarily in the benthic and hyporheic zones (benthic–hyporheic zone) of headwater streams to N_2O production occurring in the benthic zone and the water column (benthic–water column zone) of rivers, and this shift is caused by a reduction in hyporheic exchange rate with increasing stream/river discharge flows.

The work of Ocampo et al. (15) suggested interpreting NO_3 transport and transformation within a riparian zone using a Damköhler number, which is the ratio of a characteristic residence time, with importance (28) that has been documented by several empirical (5, 16, 17) and numerical (29, 30) investigations, to the characteristic time of the pertinent biogeochemical reaction. Recent investigations also proposed this approach to interpret hyporheic processes (31, 32), and they adapted it to quantify the hyporheic biogeochemical response at both bedform (33) and reach (34) scales. Here, we capitalized on these advances to depict the observed scaling effect on N_2O emissions across riverine networks (Fig. 1), and we parameterized the transformation efficiency of dissolved NO_3 to gaseous N_2O in terms of two Damköhler numbers (*Materials and Methods* and *SI Text*). In headwater streams that are typically small and shallow, microbially mediated denitrification occurs mainly within the benthic–hyporheic zone (35). Headwater stream hydrodynamics at and within the streambed (hyporheic flows) is the main factor controlling the flux of dissolved nutrients to the microbial assemblages that control biogeochemical transformations (Fig. 2). Therefore, the Damköhler number for the benthic–hyporheic zone is defined as the ratio between the median hyporheic residence time (τ_{50}), which is an index of the time that stream water spends within the hyporheic sediment, and the characteristic time of denitrification (τ_D), $\tau_D = 1/k_D$, where k_D is the denitrification reaction rate (evaluated as the ratio between the denitrification uptake rate, v_{fden}, and the mean flow depth, Y_0: $k_D = v_{fden}/Y_0$): $Da_{DHZ} = \tau_{50}/\tau_D$ (zone 1 in Fig. 2) (36). However, as stream size increases, the ratio of hyporheic to surface flow declines, which reduces the relative contribution of hyporheic zone to biogeochemical transformations (zone 2 in Fig. 2). In rivers, therefore, water column transformations combined with benthic processes at the sediment–water interface dominate denitrification, overwhelming the benthic–hyporheic contribution (zone 3 in Fig. 2). This behavior requires a different metric to describe the relevant timescale of N_2O production. We identify this metric with the time of turbulent vertical mixing, t_m, which is the average time for any neutrally buoyant particle to sweep through the entire water column because of turbulence. Thus, we introduce a unique Damköhler number for rivers, $Da_{DS} = t_m/\tau_D$, with t_m replacing τ_{50} and stating a shift from hyporheic- to water column-dominated N_2O production.

Similar to our previous work (34), we define the dimensionless flux of N_2O, F^*N_2O, as the ratio between FN_2O and the total flux per unit streambed area of dissolved inorganic nitrogen species [NO_3 and ammonium (NH_4)] in the stream ($FDIN_0$). Both reactive species are potential sources of N_2O via denitrification and nitrification, respectively (37), and may vary with time and stream (11) (Eq. **S18**). Moreover, dimensionless emissions depend on the inorganic nitrogen load through k_D, which is often parameterized as a function of the stream concentration of NO_3 (19, 20). The use of isotopic ^{15}N tracer along the LINXII Study sites (6, 10, 11) allows for separating N_2O production

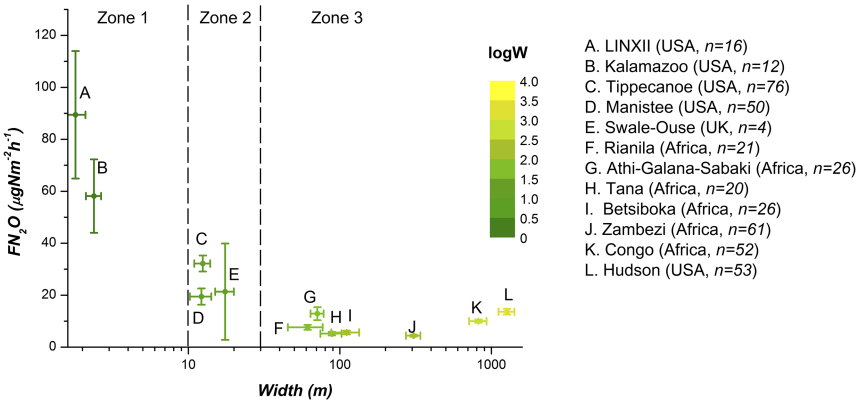

A. LINXII (USA, *n=16*)
B. Kalamazoo (USA, *n=12*)
C. Tippecanoe (USA, *n=76*)
D. Manistee (USA, *n=50*)
E. Swale-Ouse (UK, *n=4*)
F. Rianila (Africa, *n=21*)
G. Athi-Galana-Sabaki (Africa, *n=26*)
H. Tana (Africa, *n=20*)
I. Betsiboka (Africa, *n=26*)
J. Zambezi (Africa, *n=61*)
K. Congo (Africa, *n=52*)
L. Hudson (USA, *n=53*)

Fig. 1. Nitrous oxide emissions from the analyzed streams and rivers. Average N_2O emissions (FN_2O) per unit area as a function of the mean system width (W) for the analyzed streams and rivers. Zone delineation is based on FN_2O changes with stream/river size (fast change with size for zone 1, low change with size for zone 2, and no change with size for zone 3). This division is consistent with the classification proposed by the Forest Practice Code (26), Buffington and Montgomery (27), and Peterson et al. (4). Error bars represents the SE ($\pm$SE) of the mean stream width and average flux of N_2O.

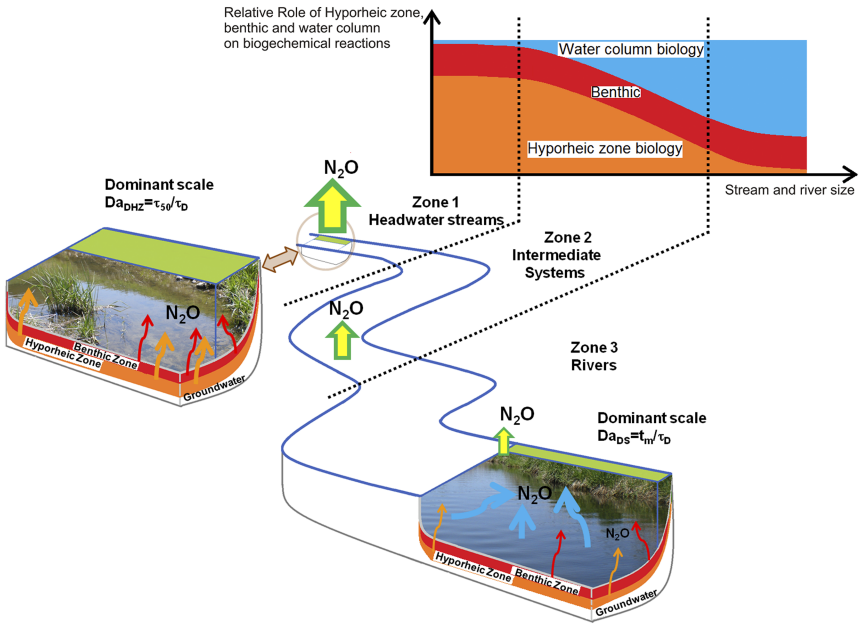

Fig. 2. Conceptual model describing the relative role of hydrodynamics and biogeochemical transformations within three zones of increasing stream size. Size of arrows indicates the magnitude of N_2O emissions per unit area from streams and rivers and the relative importance of water column (light blue), benthic (red), and hyporheic (orange) zones as sources of N_2O.

from the benthic and hyporheic zones, with the former associated with direct denitrification and the latter associated with the indirect one (6, 34) (*SI Text*). Furthermore, groundwater and water column contributions from these headwater systems were deemed negligible at the LINXII Study sites (6). Measured emissions from only the benthic zone (Fig. 3, red symbols) are one order of magnitude lower than the total emissions from both benthic and hyporheic zones (Fig. 3, orange symbols), stating the relative importance of the hyporheic zone contribution in headwater streams (zone 1 in Fig. 2). The power law relationships reported in Fig. 3 shown by red and orange lines are obtained by regression with the experimental LINXII Study data and suggest that hydromorphological processes governing hyporheic exchange also influence processes within the benthic zone. They have similar scaling patterns, with experimental data ranging more than five log scales regardless of biome, LULC type, stream morphology, stream size, and climatic conditions (Fig. 3) and effects that are accounted in the proposed dimensionless framework via $FDIN_0$, k_D, and τ_{50}, with k_D linked to biochemistry and τ_{50} linked to stream hydraulic and morphology (34, 36) (*Materials and Methods* and *SI Text*). This linkage confers predictability to the above relationships provided that $FDIN_0$ is known. The same analysis applied to N_2O flux from the benthic–hyporheic zone in the Kalamazoo River watershed (19, 20) shows a similar scaling with Da_{DHZ} for F^*N_2O (Fig. 3, green dashed line), which is not statistically different from the orange line in Fig. 3 [analysis of covariance (ANCOVA) analysis $F_{value} = 0.068 < F_{crit} = 4.259$ and $P = 0.796 > 0.05$]. Thus, we combine the LINXII Study and Kalamazoo River data and define the following power law (black solid line in Fig. 3): $F^*N_2O = 1.55 \times 10^{-7}(Da_{DHZ})^{0.43}$ and $r^2 = 0.48$, which we identify as the upper N_2O emission potential (upper bound) from headwater streams caused by processes occurring in both the hyporheic and benthic zones, whereas the production from only the benthic zone provides the lower N_2O emission potential (lower bound) (red solid line in Fig. 3). We expect that these two dimensionless power laws are globally applicable at the watershed and larger scale, because the use of Da_{DHZ} captures both the advective and biogeochemical scaling of N_2O production at the reach scale, whereas the effect of water temperature can be accounted for with an Arrhenius-like relationship when quantifying the N_2O flux from F^*N_2O. We test their generality with all study reaches (more than 400 worldwide), excluding those used in their derivation (LINXII Study, 16 streams, and Kalamazoo River, 12 streams). Therefore, N_2O emissions from headwater streams in zone 1 within a riverine network (compare Figs. 3 and 4*A*) can be computed as the product of the total mass flux of inorganic nitrogen load ($FDIN_0$) and F^*N_2O provided by the upper-bound power law model as a function of Da_{DHZ} (black line in Fig. 3). We found this power law valid for all of the headwater streams of the watersheds

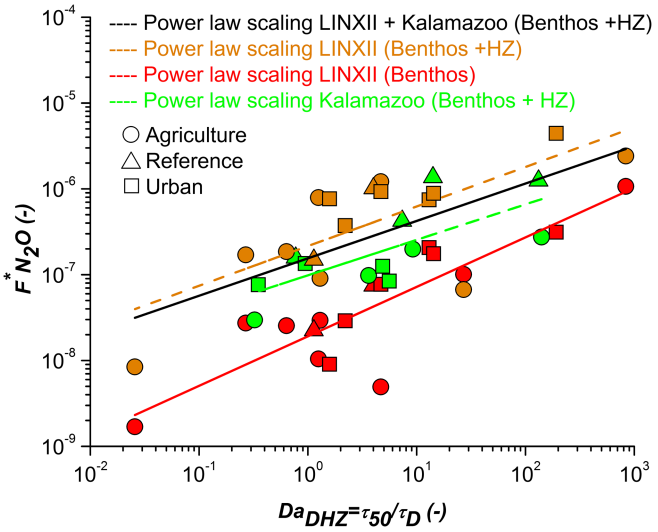

Fig. 3. Dimensionless flux of N_2O (F^*N_2O) as a function of the denitrification Damköhler number (Da_{DHZ}) in the LINXII Study (n = number of streams, $n = 16$) and the Kalamazoo River (Michigan; $n = 12$) streams. F^*N_2O resulting from the production of N_2O within only the benthic zone of the LINXII Study streams is shown with red symbols; the power law regression of these data is shown with the red solid line [$F^*N_2O = 1.91 \times 10^{-8}(Da_{DHZ})^{0.57}$, $r^2 = 0.75$]. Emissions from the benthic–hyporheic zone (combined contribution of both zones, Benthos + HZ) are in orange symbols, and their power regression is shown as the orange dashed line [$F^*N_2O = 2.15 \times 10^{-7}(Da_{DHZ})^{0.46}$, $r^2 = 0.54$]. Emissions from the benthic–hyporheic zone of the Kalamazoo streams scale with Da_{DHZ} [$F^*N_2O = 9.83 \times 10^{-8}(Da_{DHZ})^{0.41}$, $r^2 = 0.54$] as shown by the green line. Because these two relationships (dashed orange and green lines) are not significantly different, we fitted both datasets with a power law [$F^*N_2O = 1.55 \times 10^{-7}(Da_{DHZ})^{0.43}$, $r^2 = 0.48$; black line], which quantifies N_2O emissions from headwaters.

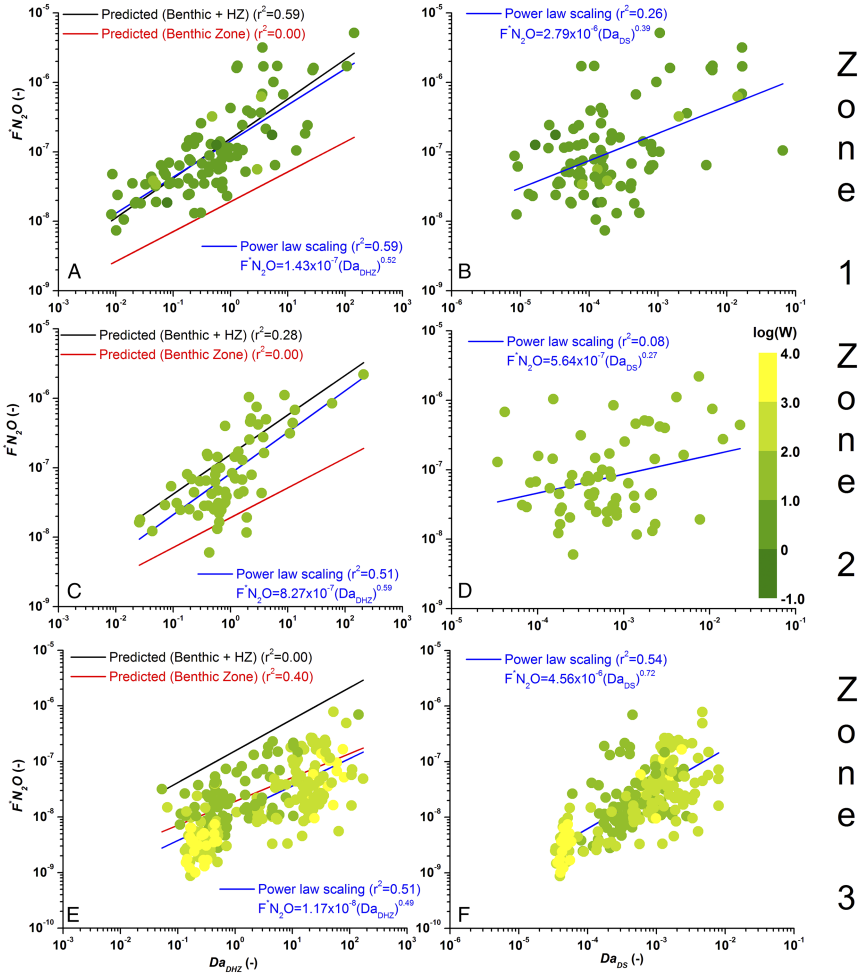

Fig. 4. Dimensionless flux of N_2O (F^*N_2O) as a function of the two Damköhler numbers, reflecting processes occurring within the benthic–hyporheic zone and the water column. None of the streams (circles), shown colored by reach width with the width increasing from green to yellow, were used in deriving the upper (black lines) and lower bounds (red lines) in *A*, *C*, and *E*. *A*, *C*, and *E* consider the scaling of F^*N_2O as a function of Da_{DHZ} for zones 1–3, respectively. Black lines represent the scaling obtained in Fig. 3 by fitting the power law to the LINXII Study and Kalamazoo River data [n = number of streams, $n = 28$; $F^*N_2O = 1.55 \times 10^{-7}(Da_{DHZ})^{0.43}$]. Red lines represent the scaling obtained by fitting the power law to the LINXII Study data ($n = 16$) considering only benthic emissions (red line in Fig. 3) [$F^*N_2O = 1.91 \times 10^{-8}(Da_{DHZ})^{0.57}$], and blue lines represent the fitting of the power law with all of the data shown. *B*, *D*, and *F* show the scaling of F^*N_2O as a function of Da_{DS} for zones 1–3 (n = 91, 66, and 247, respectively). The blue continuous lines represent the fitting of a power law with all of the data shown by circles in the graph.

analyzed in this study regardless of biomes, LULC, or climatic conditions (in Fig. 4*A*, notice the higher r^2 of 0.59 when applied for all studied headwater streams without including those used to derive the upper-bound power law relationship in Fig. 3). The regression of a power law to all of the available data (blue line in Fig. 4*A*) is also not statistically different (ANCOVA analysis $F_{value} = 0.0 < F_{crit} = 3.89$ and $P = 1 > 0.05$) from the upper-bound power law (black lines in Figs. 3 and 4*A*) and maintains the same r^2. Thus, we suggest that the upper-bound power law could be widely applicable to streams across the globe because of the breath of our data. Some unexplained variance is likely caused by N_2O originating from groundwater and terrestrial sources or nitrification/denitrification of groundwater NH_4. Our model assumed that the main source of N_2O resulted from transformations of dissolved inorganic nitrogen (NO_3 plus NH_4) present in the stream without distinguishing the source of dissolved inorganic nitrogen (e.g., groundwater, runoff, or atmospheric deposition). As such, we may partially account for NH_4 of groundwater origin if nitrification occurs within the stream via transformation in the water column, benthic, or hyporheic zone. Another potential source of error is that we do not account explicitly for hyporheic downwelling fluxes that control the amount of reactants delivered to the sediment. These fluxes depend on the same hydromorphological parameters that characterize τ_{50}, and thus, we implicitly, although partially, account for downwelling fluxes via τ_{50}, because there is an inverse relationship between τ_{50} and mean hyporheic downwelling flux.

As stream/river size increases, the relative contribution of the hyporheic zone to N_2O emissions in relation to the benthos and water column declines; consequently, our conceptual model predicts a decline in dimensionless emissions, F^*N_2O (compare Fig. 4 *A*, *C*, and *E*). Notice that colors of the symbols in Fig. 4 vary from green to yellow as the width of the system increases from streams to rivers. The coefficient of determination of the upper-bound power law model, which includes both benthic and hyporheic zones (in Fig. 4, the black lines are the same as in Fig. 3), declines moving from headwater streams (Fig. 4*A*, $r^2 = 0.59$) to intermediate systems (Fig. 4*C*, $r^2 = 0.28$) and rivers (Fig. 4*E*, $r^2 = 0$). This decrease suggests a shift in processes controlling N_2O production. When the data are fitted, r^2 rises again, but the resulting regression curves, shown in blue in Fig. 4 *C* and *E*, increasingly deviate from the power law model of zone 1

(upper bound) (black line in Fig. 3) as stream and river size increases (moving from Fig. 4 *A*, *C*, and *E*) and approaches the lower-bound power law model (Fig. 3, red line with r^2 of 0.40 when applied for all studied rivers, of which none were used for its derivation). The fitted blue line in Fig. 4*E* and the lower-bound power law (red line in Fig. 4*E*), which was derived without the contribution of the hyporheic zone (Fig. 3), are not statistically different (ANCOVA analysis $F_{value} = 0 < F_{crit} = 3.86$ and $P = 1 > 0.05$), which suggests that hyporheic processes have a negligible contribution to N_2O emissions in rivers. Conversely, a power law, $F^*N_2O = c_1(Da_{DS})^b$, where Da_{DS}, encapsulating hydrodynamic and biochemical processes occurring in the benthic–water column environment, replaces Da_{DHZ} fitted to the experimental data separately (Fig. 4 *B*, *D*, and *F*), shows very low-determination coefficients in headwater and intermediate systems (Fig. 4 *B*, $r^2 = 0.26$ and *D*, $r^2 = 0.08$) but a value comparable with that in Fig. 4*A* for rivers ($r^2 = 0.54$ in Fig. 4*F*). Consequently, N_2O emissions from rivers scale with Da_{DS} (which is defined by replacing the hyporheic residence time with the residence time in the water column) better than with Da_{DHZ} (compare Fig. 4 *E* and *F*).

We suggest that the contribution of the water column to N_2O emissions increases from streams to rivers as an effect of an increase in suspended particle loads. Denitrification has been shown to occur within anoxic microsites associated with suspended sediments located throughout the well-mixed water column (38) typical of river systems. Contrary to existing modeling and empirical approaches (12, 34, 36), which suggest that the hyporheic zone or benthos is the primary source of N_2O regardless of stream and river size, our data show a systematic shift from predominantly hyporheic–benthic N_2O production in streams to predominantly benthic–water column production in rivers.

Using a metaanalysis of all available data collected by us and previously published, we show that this shift is controlled by key hydrodynamic and biogeochemical parameters that effectively explain the observed decline of N_2O emissions per unit area as the stream/river size increases. We used hydrodynamic parameters typically collected in the field for morphologic classification: the reach-scale mean flow velocity (V), the hydraulic depth (Y_0), the mean channel width (W), the channel slope (s_0), the median grain size (d_{50}), and the type of bed forms. When not measured or observed in the field, we estimated these quantities by means of morphological relationships as a function of drainage area and water discharge (39–41) (Table S5) or using information extracted from remote sensing and Digital Terrain Map analysis (chiefly for W and s_0). In addition, we used morphological relationships on bed-form stability to characterize bed-form morphology and d_{50} (42, 43) when not observed in the field. Successively, we used these parameters to quantify t_m (Eq. **S1**) or τ_{50} (Eq. **S4** shows dune morphology, and Eq. **S7** shows pool-riffle morphology). The biogeochemical parameters are k_D, which we evaluated in the field or derived from NO_3 concentrations measurements (Table S3), and NO_3 and NH_4 concentrations. All of these quantities vary among reaches belonging to the same river system as noted in Tables S2 and S3, which report the minimum and maximum values for each river system as well as the variability of Da_{DHZ} and Da_{DS}, which depends on variation in morphological and biogeochemical parameters (Table S3). This variability results from natural variation in both hydraulics and biogeochemical parameters among reaches and may explain, at least partially, the scatter observed in Figs. 3 and 4, but it does not represent the effect of parameter uncertainty or within-reach variability, which we do not consider here. N_2O emissions per unit area are predictable and greater, for a given nutrient load, in headwater streams compared with rivers, in part because of the contribution of the hyporheic zone. Headwater streams are important sources of N_2O emissions along riverine networks resulting from a combination of significant contact time with the bioreactive benthic–hyporheic zone and significant surface–subsurface exchange of water and solutes (4, 18) as well as their relative predominance in river networks. In contrast, as streams transition to rivers, the contribution of the hyporheic zone declines, and benthic–water column contribution dominates. Thus, headwater streams may have a disproportionate impact on annual N_2O emissions, especially if they drain agricultural or urban LULC type, because they also represent the greatest proportion of riverine network drainage length (4).

We unveiled the primary scaling factors governing riverine N_2O emissions and provide a predictive tool that can be applied worldwide to quantify N_2O emissions from riverine environments across scales from headwater streams ($Q < 0.2$ m^3/s) to rivers ($Q \approx 19,000$ m^3/s) draining a variety of biomes, LULC types, and climatic conditions through accessible reach-scale geochemical measurements (i.e., stream temperature and NO_3 concentration) and hydromorphological parameters (i.e., stream morphology, mean flow depth, velocity, slope, and channel width) (*SI Text*). Our scaling laws allow one to quantify N_2O emissions at the watershed scale using geographic information system analyses of stream morphology (44) and readily available measurements of nitrate and ammonium, which can be distributed throughout the river network, both in space and through time (45). This approach requires robust hyporheic models linked to hydromorphological information. These models are not currently available for cascade, step-pool, and plane-bed morphologies (34), which are common in small headwater streams (27). Consequently, there is a need for research to define these relationships, include them in network-scale hyporheic models, and quantify *Da* numbers, such as in the project Networks with Exchange and Subsurface Storage (12) to predict reach-scale N_2O emissions. Furthermore, the above evidences of the role of river morphology in controlling N_2O emissions may contribute to improvement of conceptual models by considering stream morphology and constraining and linking the role of the different parts of the stream/river reach (e.g., hyporheic zone, benthic zone, the water column, and also the riparian zone). This scaling framework actively quantifies the impact of human activity and natural forcing through τ_{50}, a function of river morphology and hydrology (46), which may change because of climate change, water extraction, sediment transport regime, and land use, and τ_D, which accounts for land use land cover, and therefore, water quality. Water temperature effects on N_2O emissions can be also accounted by scaling the dimensionless value with an Arrhenius-type equation. Thus, the framework can be used to quantify N_2O emissions under different scenarios and treatments, such as watershed-scale changes in land use and water management or how changing climate influences biogeochemical outcomes. Consequently, it provides the needed feedback among climate, LULC, and water management to help quantify human impact on climate change at the global scale.

Materials and Methods

The dimensionless flux of N_2O from riverine networks is parameterized with a Damköhler number that represents the ratio between the characteristic residence time within the denitrifying zones (benthic, hyporheic, and water column) and the characteristic time of the biogeochemical reaction. For the purpose of this model, the characteristic time of the biogeochemical reaction is the time of denitrification, τ_D, and it is defined as the inverse of the denitrification reaction rate k_D ($\tau_D = 1/k_D = Y_0/v_{fden}$) (details on the calculation of τ_D are in *SI Text*), whereas the characteristic residence time within the denitrifying zones changes along the riverine network according to the riverine environments that mainly control this biogeochemical process.

In headwater streams, a robust estimator of the time that a solute molecule is exposed to the denitrifying environment is the median hyporheic residence time (τ_{50}), which is the time at which 50% of stream water that entered the streambed sediment is still within the hyporheic zone. Its value is a function of streambed morphology, surface hydraulics, and groundwater table (details on the calculation of τ_{50} are in *SI Text*). Consequently, it accounts for the impact of external forcing on stream physical conditions, such as human water management, or climate change on discharge and sediment transport. Changes in both discharge and sediment input caused by climate change affect bed-form type and shape. This forcing also includes LULC, biome, and climatic conditions. Therefore, the Damköhler number for the benthic–hyporheic zone is defined as the ratio

between the characteristic time controlling hyporheic residence time and the characteristic time controlling the denitrification process:

$$Da_{DHZ} = \frac{\tau_{50}}{\tau_D}. \quad [1]$$

Values of $Da_{DHZ} < 1$ suggest that the system is limited by the denitrification rate (i.e., low k_D) or short residence time (small τ_{50}). Conversely, $Da_{DHZ} > 1$ suggests high denitrification efficiency (high k_D) or long residence time (large τ_{50}) (zone 1 in Fig. 2).

As stream size increases, the ratio of hyporheic to surface flow declines in favor of a gradual contribution of the benthic–water column in controlling denitrification (zone 2 in Fig. 2). Rivers are turbulent systems in which dissolved solutes and particles are vertically mixed throughout the water column (47), thus requiring a different metric to describe the relevant timescale of N_2O production. We identify this metric with the time of turbulent vertical mixing, t_m, which is the average time for any neutrally buoyant particle to sweep through the entire water column because of turbulence (details on the calculation of t_m are in *SI Text*). Thus, we introduce a unique Damköhler number for rivers as follows:

$$Da_{DS} = \frac{t_m}{\tau_D}, \quad [2]$$

where the median residence time in the hyporheic zone, τ_{50}, is replaced by t_m, stating a shift from hyporheic- to water column-dominated N_2O production. When $Da_{DS} < 1$ ($t_m < \tau_D$), the timescale for the vertical mixing is less than that of denitrification; therefore, the production of N_2O is chiefly controlled by microbial activity. In contrast, when $Da_{DS} > 1$ ($t_m > \tau_D$), the production of N_2O is controlled by hydrodynamics, which determines solute mixing throughout the water column, thereby influencing the contact time with microbial denitrifiers carried by suspended particles.

All data reported in the paper are reported in *SI Text*.

ACKNOWLEDGMENTS. This research is supported by National Science Foundation Awards 1344661 and 1344602 and by the European Communities 7th Framework Programme under Grant Agreement 603629-ENV-2013-6.2.1-Globaqua. Any opinions, conclusions, or recommendations expressed in this material are those of the authors and do not necessarily reflect the views of the supporting agencies.

1. Syakila A, Kroeze C (2011) The global nitrous oxide budget revisited. *Greenhouse Gas Meas Manage* 1:17–26.
2. Harvey JW, Böhlke JK, Voytek MA, Scott D, Tobias CR (2013) Hyporheic zone denitrification: Controls on effective reaction depth and contribution to whole-stream mass balance. *Water Resour Res* 49:6298–6316.
3. Seitzinger SP (1988) Denitrification in freshwater and coastal marine ecosystems: Ecological and geochemical significance. *Limnol Oceanogr* 33:702–724.
4. Peterson B, et al. (2001) Control of nitrogen export from watershed by headwater streams. *Nature* 292:86–89.
5. Zarnetske JP, Haggerty R, Wondzell SM, Baker MA (2011) Dynamics of nitrate production and removal as a function of residence time in the hyporheic zone. *J Geophys Res* 116:G01025.
6. Beaulieu JJ, et al. (2011) Nitrous oxide emission from denitrification in stream and river networks. *Proc Natl Acad Sci USA* 108:214–219.
7. Boano F, et al. (2014) Hyporheic flow and transport processes: Mechanisms, models, and biogeochemical implications. *Rev Geophys* 52:603–679.
8. Rosamond MS, Thuss SJ, Schiff SL (2012) Dependence on riverine nitrous oxide emissions on dissolved oxygen levels. *Nat Geosci* 5:715–718.
9. Weiss RF, Price BA (1980) Nitrous oxide solubility in water and seawater. *Mar Chem* 8:347–359.
10. Mulholland PJ, et al. (2008) Stream denitrification across biomes and its response to anthropogenic nitrate loading. *Nature* 452:202–206.
11. Hall RO, et al. (2009) Nitrate removal in stream ecosystems measured by ^{15}N addition experiments: Total uptake. *Limnol Oceanogr* 54:653–665.
12. Gomez-Velez JD, Harvey JW (2014) A hydrogeomorphic river network model predicts where and why hyporheic exchange is important in large basins. *Geophys Res Lett* 41:6403–6412.
13. Venkiteswaran JJ, Rosamond MS, Schiff SL (2014) Nonlinear response of riverine N_2O fluxes to oxygen and temperature. *Environ Sci Technol* 48:1566–1573.
14. Turner PA, et al. (2015) Indirect nitrous oxide emissions from streams within the US Corn Belt scale with stream order. *Proc Natl Acad Sci USA* 112:9839–9843.
15. Ocampo CJ, Oldham CE, Sivapalan M (2006) Nitrate attenuation in agricultural catchments: Shifting balances between transport and reaction. *Water Resour Res* 42:W01408.
16. Gu CH, Hornberger GM, Mills AL, Herman JS, Flewelling SA (2007) Nitrate reduction in streambed sediments: Effects of flow and biogeochemical kinetics. *Water Resour Res* 43:W12413.
17. Pinay G, O'Keefe TC, Edwards RT, Naiman RJ (2009) Nitrate removal in the hyporheic zone of a salmon river in Alaska. *River Res Appl* 25:367–375.
18. Alexander RB, Smith RA, Schwarz GE (2000) Effect of stream channel on the delivery of nitrogen to the Gulf of Mexico. *Nature* 403:758–761.
19. Beaulieu JJ, Arango CP, Hamilton SK, Tank JL (2008) The production and emission of nitrous oxide from headwater streams in the Midwestern United States. *Glob Chang Biol* 14:878–894.
20. Beaulieu JJ, Arango CP, Tank JL (2009) The effects of season and agriculture on nitrous oxide production in headwater streams. *J Environ Qual* 38:637–646.
21. Pattinson SN, García-Ruiz R, Whitton BA (1998) Spatial and seasonal variation in denitrification in the Swale-Ouse system, a river continuum. *Sci Total Environ* 210/211:289–305.
22. García-Ruiz R, Pattinson SN, Whitton BA (1999) Nitrous oxide production in the river Swale-Ouse, North-East England. *Water Res* 33:1231–1237.
23. Borges AV, et al. (2015) Globally significant greenhouse-gas emissions from African inland waters. *Nat Geosci* 8:637–642.
24. Cole JJ, Caraco NF (2001) Emissions of nitrous oxide (N_2O) from a tidal, freshwater river, the Hudson river, New York. *Environ Sci Technol* 35:991–996.
25. Caraco NF, et al. (1997) Zebra mussel invasion in a large, turbid river: Phytoplankton response to increased grazing. *Ecology* 78:588–602.
26. Forest Practice Code (1996) *Channel Assessment Procedure Field Guidebook in Forest Practice Code* (British Columbia Ministry of Forest, Vancouver), pp 1–95.
27. Buffington JM, Montgomery DR (2013) Geomorphic classification of rivers. *Treatise on Geomorphology*, eds Shroder J, Whol E (Academic, San Diego), pp 730–767.
28. Gooseff MN (2010) Defining hyporheic zones Advancing our conceptual and operational definitions of where stream water and groundwater meet. *Geogr Compass* 4:945–955.
29. Cardenas MB, Cook PLM, Jiang H, Traykovski P (2008) Constraining denitrification in permeable wave-influenced marine sediment using linked hydrodynamic and biogeochemical modeling. *Earth Planet Sci Lett* 275:127–137.
30. Boano F, Demaria A, Revelli R, Ridolfi L (2010) Biogeochemical zonation due to intrameander hyporheic flow. *Water Resour Res* 46:W02511.
31. Zarnetske JP, Haggerty R, Wondzell SM, Bokil VA, González-Pinzón R (2012) Coupled transport and reaction kinetics control the nitrate sources-sink function of hyporheic zones. *Water Resour Res* 48:W11508.
32. Abbott BW, et al. (2016) Using multi-tracer inference to move beyond single-catchment ecohydrology. *Earth Sci Rev* 160:19–42.
33. Marzadri A, Tonina D, Bellin A (2012) Morphodynamic controls on redox conditions and on nitrogen dynamics within the hyporheic zone: Application to gravel bed rivers with alternate-bar morphology. *J Geophys Res* 117:G00N10.
34. Marzadri A, Tonina D, Bellin A, Tank JL (2014) A hydrologic model demonstrates nitrous oxide emissions depend on streambed morphology. *Geophys Res Lett* 41:5484–5491.
35. Reisinger AJ, Tank JL, Rosi-Marshall EJ, Hall RO, Baker MA (2015) The varying role of water column nutrient uptake along river continua in contrasting landscapes. *Biogeochemistry* 125:115–131.
36. Gomez-Velez JD, Harvey JW, Cardenas MB, Kiel B (2015) Denitrification in the Mississippi river network controlled by flow through river bedforms. *Nat Geosci* 8:941–945.
37. Mulholland PJ, et al. (2004) Stream denitrification and total nitrate uptake rates measured using a field ^{15}N tracer addition approach. *Limnol Oceanogr* 49:809–820.
38. Liu T, Xia X, Liu S, Mou X, Qiu Y (2013) Acceleration of denitrification in turbid rivers due to denitrification occurring on suspended sediment in oxic waters. *Environ Sci Technol* 47:4053–4061.
39. Leopold LB, Maddock T (1953) *The Hydraulic Geometry of Stream Channels and Some Physiographic Implications* (US Government Printing Office, Washington, DC), Tech Rep 57.
40. Rhoads BL (1991) A continuously varying parameter model of downstream hydraulic geometry. *Water Resour Res* 27:1865–1872.
41. Raymond PA, et al. (2012) Scaling the gas transfer velocity and hydraulic geometry in streams and small rivers. *Limnol Oceanogr Fluids Environ* 2:41–53.
42. Yalin MS (1964) Geometrical properties of sand waves. *Proc Amer Soc Civ Eng, J Hydraul Div* 90:105–119.
43. Ikeda S (1984) Prediction of alternate bar wavelenght and height. *J Hydraul Eng* 110:371–386.
44. Buffington JM, Montgomery DR, Greenberg HM (2004) Basin-scale availability of salmonid spawning gravel as influenced by channel type and hydraulic roughness in mountain catchments. *Can J Fish Aquat Sci* 61:2085–2096.
45. McGuire KJ, et al. (2014) Network analysis reveals multiscale controls on streamwater chemistry. *Proc Natl Acad Sci USA* 111:7030–7035.
46. Goode JR, et al. (2013) Potential effects of climate change on streambed scour and risks to salmonid survival in snow-dominated mountain basins. *Hydrol Process* 27: 750–765.
47. Rutherford JC (1994) *River Mixing* (Wiley, Chichester, UK).
48. Jobson AE, Sayre WW (1970) Vertical transfer in open channel flow. *J Hydraul Div* 96:703–724.
49. Salarashayeri AF, Siosemarde M (2012) Prediction of soil hydraulic conductivity from particle-size distribution. *World Acad Sci Eng Technol* 61:454–458.
50. Elliott AH, Brooks NH (1997) Transfer of nonsorbing solutes to a streambed with bed forms: Theory. *Water Resour Res* 33:123–136.
51. Shen HV, Fehlman HM, Mendoza C (1990) Bed form resistances in open channel flows. *J Hydraul Div* 116:799–815.
52. Jähne B, et al. (1987) On the parameters influencing air-water gas exchange. *J Geophys Res* 92:1937–1949.
53. Wanninkhof R (1992) Relation between wind speed and gas exchange over the ocean. *J Geophys Res* 97:7373–7382.